
European Coordination for Accelerator Research and Development

**PUBLICATION**

# ATF2 tests and CLIC IR study

Angal-Kalinin, D (Daresbury) *et al*

19 June 2014

The research leading to these results has received funding from the European Commission under the FP7 Research Infrastructures project EuCARD, grant agreement no. 227579.

This work is part of EuCARD Work Package **9: Technology for normal conducting higher energy linear accelerators**.

The electronic version of this EuCARD Publication is available via the EuCARD web site <http://cern.ch/eucard> or on the CERN Document Server at the following URL : <http://cds.cern.ch/record/1710304

Grant Agreement No: 227579

# EuCARD

European Coordination for Accelerator Research and Development

Seventh Framework Programme, Capacities Specific Programme, Research Infrastructures, Combination of Collaborative Project and Coordination and Support Action

# DELIVERABLE REPORT

# ATF2 TESTS AND CLIC IR STUDY

## D9.4.1

| | |
|---|---|
| **Document identifier:** | EuCARD-Del-D9-4-1-v1 6_2013_07_13 |
| **Due date of deliverable:** | End of Month 42 (August 2012) |
| **Report release date:** | 17/07/2013 |
| **Work package:** | WP9 NCLinac |
| **Lead beneficiary:** | RHUL |
| **Document status:** | Final |

**Abstract:**

This task covered three separate subtasks dealing with ILC and CLIC beam delivery system and Interaction region studies as well as testing the tuning procedures at ATF2 final focus test facility. The proposed local chromaticity correction final focus system for both ILC as well as CLIC is being tested experimentally for the first time at ATF2, various tuning procedures have been applied to study the applicability of various procedures to the ILC and CLIC to optimize the interaction region. The CLIC IR region was studied in detail, and the impact and mitigation of CLIC detector solenoid effects on the beam orbit, coupling and extraction have been considered. The work programme of this task concentrated on central region integration of the ILC following the design changes proposed during the technical design phase of the ILC, participation in ATF2 beam tuning studies and CLIC interaction region studies.

The European Coordination for Accelerator Research and Development (EuCARD) is a project co-funded by the European Commission in its 7th Framework Programme under the Grant Agreement no 227579. EuCARD began in April 2009 and will run for 4 years.



## Delivery Slip

| | Name | Partner | Date |
|---|---|---|---|
| **Authored by** | D. Angal-Kalinin, R. Appleby, J. Jones, A. Scarfe, S. Tygier | [STFC/UMAN] | 17/01/13 |
| **Reviewed by** | J-P. Koutchouk | [CERN] | 13/03/13 Recd by authors 25/06/13 Next revised version 02/07/13 Comments recd 05/07/13 Revised version 13/07/13 |
| **Approved by WP Coordinator** | E. Jensen | [CERN] | 16/07/13 |
| **Approved by Project coordinator** | Jean-Pierre Koutchouk | | 16/07/13 |

# TABLE OF CONTENTS

# 1. EXECUTIVE SUMMARY

*CLIC PCL studies: In order to maximise the luminosity of collsions at CLIC the beams must aligned with an accuracy of a few nanometers. The collisions at the interaction point create large amount of disrupted beam that must be transported to a beam dump. This disrupted beam also carries information about the collision and so provides opportunity for measuring and optimising the beam alignment. We calculate required detector sensitivity to be sensitive to offsets causing a 10% loss in luminosity. A single photon detector placed after the intermediate dump can provide sufficient information for horizontal alignment, but it was found that multiple detectors are required for sufficient vertical resolution.*

*ILC Beam Delivery System (BDS): In order to address both a reduction in cost and a more complete and robust design approach, central integration of several systems of the Reference Design Report (RDR) was proposed by the ILC management. The motivation for this change is the simplification of the central region tunnelling and civil engineering. This modification needed changes in the electron side of the beam delivery system as the undulator to generate positrons moves in the beginning of electron BDS. A dogleg design was proposed satisfying the layout constraints whilst keeping emittance growth within acceptable limits at 1 TeV CM energy. Due to the strong focussing required in this lattice, the implications on tuning and tolerances have been presented, showing tight tolerances on the incoming dispersion, as well as the required trajectory correction. Correction of these errors using the 4 "end" dipoles in the design has shown the possibility to widen the tolerance levels significantly. Few other changes were made to the ILC BDS design to separate the machine protection and upstream polarimetry chicane. The summary of all changes to the ILC BDS lattices were summarised in a document due to proposed wind down on the linear collider activities within the UK.*

*ATF2 simulations and experimental tests: The goal of ATF2 programme is to test the proposed local chromaticity correction final focus system for future linear colliders (ILC and CLIC) experimentally for the first time. Various orbit correction methods and tuning procedures were applied to study the applicability of various procedures to the ILC and CLIC to optimize the interaction region. The staff participated in beam shifts at ATF2 till Autumn 2010 but could not continue participation in ATF2 due to reduced UK participation in linear collider activities since Autumn 2010. During participation in ATF2, novel algorithms have been generated and simulated, that will provide guidance for the future linear collider. The international collaborators are continuing tests at ATF2 in 2012/13 to achieve the final goal to minimize and measure a vertical beam size of ~35 nm level at the interaction point.*

*CLIC IR solenoid compensation : The detector solenoid of CLIC causes a range of aberrations on the beam at the interaction point, particularly due to its overlap with the final focus magnets. These effects are corrected using anti-solenoid correction coils on the final quadrupole before the collision point. In this note, we use the interaction region beam dynamics code IRSYN to compute the impact of the SiD solenoid on the beam and benchmark the anti-solenoid correction. We find the correction is achieved, with a small residual amount of beam aberration which is correctable using the beam delivery system. This provides a validation of the correction and a benchmark of IRSYN to existing codes.*

# 2. INTRODUCTION

The Cockcroft Institute at Manchester and Daresbury have contributed to the ILC and CLIC beam delivery system and extraction line designs since 2003 and have developed several tuning procedures to achieve ultralow beam sizes (~nm) at the interaction point. ATF2 final focus test facility at KEK provides a unique test facility to experimentally test some of these procedures and use this knowledge to optimize the designs of the interaction region of both ILC and CLIC. The EuCARD work programme concentrated on the testing of different tuning procedures and tuning knobs at ATF2 to achieve the vertical beam size down to 35nm. Even though the final goal is not yet met, several modifications have been done in the ATF2 beam line to progress towards this goal. The design changes and simulation knowledge of ILC and CLIC BDS and post collision line undertaken during EuCARD project and the simulation and experimental work carried out at ATF2 have provided better insight of beam dynamics issues to achieve better understanding of these designs and will be useful in future when linear collider project based on similar final focus system will become a reality.

# 3. LUMINOSITY MONITORING IN THE CLIC POST COLLISION LINE

## 3.1. COLLISION PRODUCTS

CLIC collides 1.5 TeV electron and positron bunch trains with 312 bunches of $3.72 \times 10^9$ particles at 50 Hz, giving a total power of 14 MW per beam. To achieve a design luminosity of $5.9 \times 10^{34}$ $cm^{-2}s^{-2}$ the beams must be squeezed to an RMS size of 40 nm horizontally and 1 nm vertically. The Post Collision Line (PCL) takes the disrupted beam and collision products from the Interaction Point (IP) to the main dump. There are opportunities for determining collision parameters from measurements of the collision products in the PCL.

Due to the small bunch sizes there is a large amount of disruption to the beam at the IP. In a head on collision approximately 30 % of the beam energy is converted to beamstrahlung photons, leaving the disrupted beam with a wide energy spread. In the strong EM field of the bunch these photon can form coherent $e^+e^-$ pairs. Additional $e^+e^-$ pairs and photons are created from incoherent processes and Bhabha scattering.

The collision was modelled with the GUINEA-PIG [1] monte-carlo code and data files containing the outgoing particles were provided by [2]. Simulations used 150000 macroparticles to represent the $3.72 \times 10^9$ particles in the bunch. Table 1 shows the main collision products.

| Product | Particles per crossing | Power |
|---|---|---|
| Spent Beam | $3.720 \times 10^9$ | 10.07 MW |
| Beamstrahlung photons | $7.681 \times 10^9$ | 3.608 MW |
| Coherent same sign | $1.675 \times 10^8$ | 130.1 kW |
| Coherent opposite sign | $1.675 \times 10^8$ | 128.2 kW |
| Radiative Bhabhas | $5 \times 10^5$ | 1 kW |
| Incoherent pairs | | 78 W |

*Table 1: Main collision products*

Due to the small size of the beams at the interaction point (IP), the luminosity falls off sharply if the beams are offset, as shown in Figure 1. Fitting a Gaussian gives a sigma of 2.89 nm for vertical and 61.22 nm for horizontal offsets. The difference is due to the flat shape of the beam. Luminosity will drop by 10% for offsets of 1.32 nm vertically and 28.1 nm horizontally.

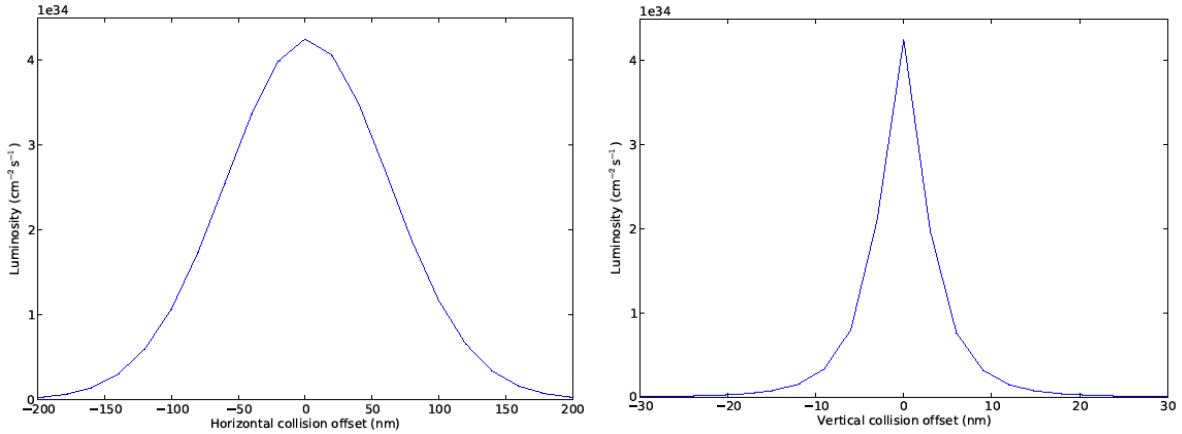


*Figure 1. Collision luminosity as a function of collision offset, horizontally (left) and vertically (right).*

The beamstrahlung is strongest not for a direct head on collision, but for a 9 nm vertical offset. This is where the beams see the strongest field of the other beam. Figure 2 shows how the photon count varies with horizontal and vertical offset, and figure 3 shows the same for power.

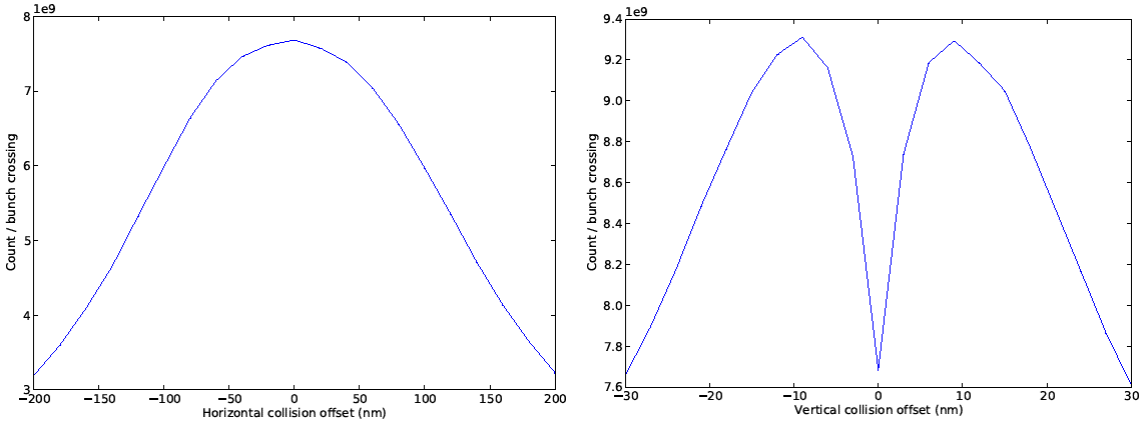


*Figure 2. Count of photons created at the IP as a function of collision offset horizontally (left) and vertically (right).*

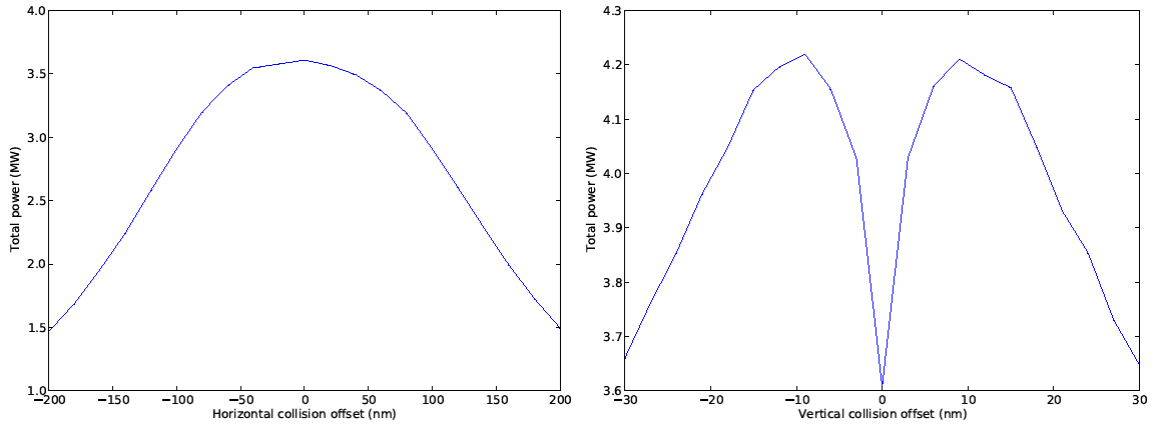


*Figure 3. Power of photons created at the IP as a function of collision offset horizontally (left) and vertically (right).*

The collision offset also affects the angle of the photon cone. Horizontal offsets lead to an angle in *x* and vertical offsets to an angle in *y* as shown in figure 4. Horizontal offsets do not have a strong effect on *y* and vertical offsets do not strongly affect *x*.

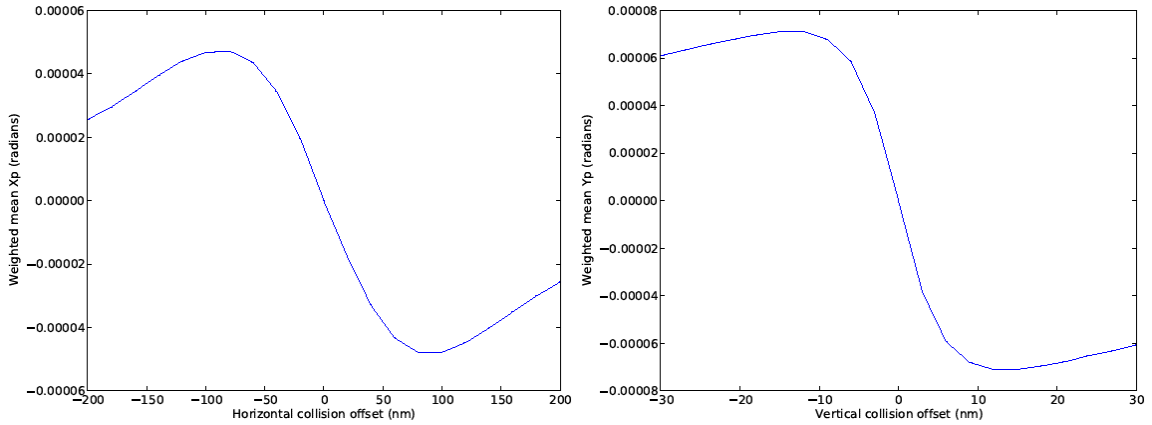


*Figure 4. Weighted mean angle of photons created at the IP as a function of collision offset horizontally (left) and vertically (right).*

The signal seen at a photon detector will depend on the intensity, distribution and angle of the photon cone, and so will vary with the collision offsets. It is possible to work back from the signal to derive the collision offsets, and so optimise the crossing to maximise luminosity.

## 3.2. POST COLLISION LINE GEOMETRY

The PCL is designed to carry the outgoing collision products so that they can be safely dumped. The layout is described in detail in [3], though some details have been updated, most notably dump has been moved to 315 m from the IP. Figure 5 shows a schematic of the layout.

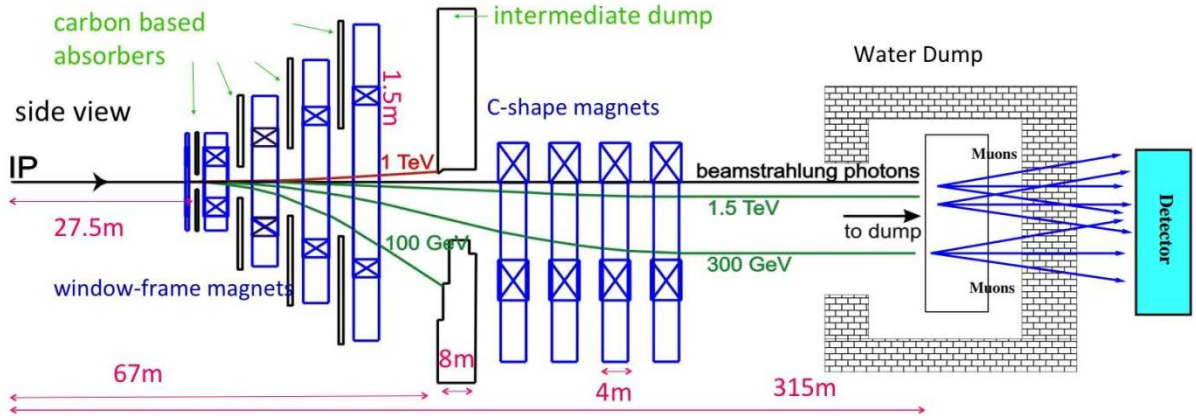


*Figure 5. Post collision Line layout*

The crossing angle at the IP is 20 mrad, so it is not possible to place magnets close to the IP without interfering with incoming beam line. The first element in the PCL is at 27.5 m. The main dump must be placed far enough from the IP to allow an uncollided beam to spread and to minimise secondary particles produced in the dump returning to the particle physics detector. The main dump is placed at 315 m from the IP. Two dipole sections are included in the line, this allows separation of the positive, negative and uncharged components of the beam, and also to provide dispersion, to further spread the beam on the dump. The first set of dipoles bend the disrupted beam downwards, and the second set return it to horizontal.

The collision products have a wide energy range, and so it is necessary to do some collimation of the lower energy particles before the main dump. This is done with masks between the magnets in the first bend, and an intermediate dump between the two bends. Same sign particles with less than 83 % of 1.5 TeV initial momentum and opposite sign particles up to the full momentum hit the intermediate dump, as shown in figure 5. While the higher energy particles and the beamstrahlung photons which carry around 98 % of the power, pass through to be transported to the main dump.

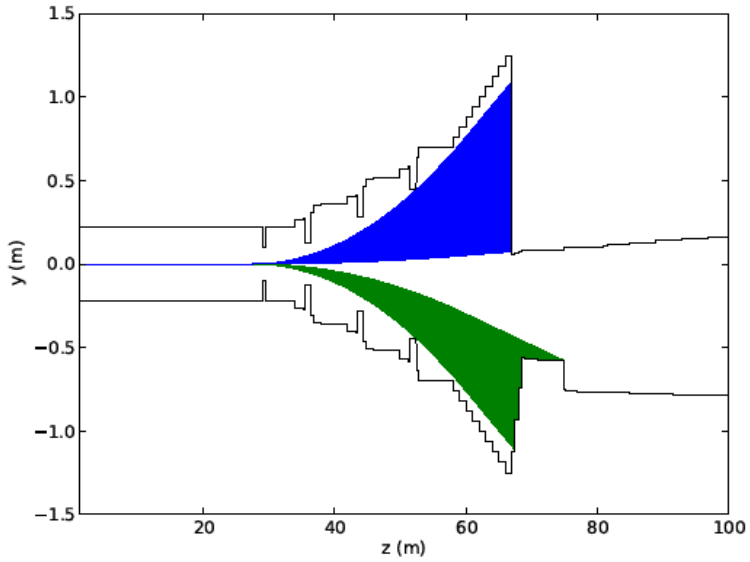


*Figure 6. Same (green) and opposite (blue) sign low energy particles are bent to hit the intermediate dump. Vertical extent of the aperture is shown in black.*

### 3.2.1. Magnets

The first bend consists of five 1 T window dipole magnets. The first two, 1A and 1B, have lengths 0.5 and 3 m respectively, and the others are 4 m long. They are positioned from 27.5 through to 58 m from the IP. Between them are four masks, the first is 0.5 m and the other three are 0.9 m long. Beyond the intermediate dump there are four 4 m long 1 T dipoles. These are C-shaped and positioned from 77 to 105 m.

More details of the geometry of the PCL are given in the appendix.

## 3.3. FLUKA MODEL

The PCL was modelled using FLUKA 2011 [4,5]. The geometry contains the beam pipe, the magnets including coils, collimation masks, intermediate and final dump, the tunnel wall and floor, the air in the tunnel and the soil outside the tunnel. The beam pipe is an elliptic cylinder up to the intermediate dump, and composed of two half elliptic cylinders and a straight section after the dump. The changes in beam pipe size along *z* are modelled as many small steps.

FLUKA was run with the new default settings with production cuts set to be equivalent to a 10 cm range cut in GEANT4. The cut values are shown in table 2. The `EMFCUT` keyword was used to implement the production cuts. FLUKA uses the electron cut value for both electrons and positrons. Photon nuclear interactions were not enabled, as they significantly increase simulation time and gave very small power fluxes at the detector sites.

| Material | Gamma | Electron | Positron |
|---|---|---|---|
| VACUUM | 990 | 990 | 990 |
| AIR | $1.20302\times10^{3}$ | $88.1421\times10^{3}$ | $86.9654\times10^{3}$ |
| Concrete | $62.9882\times10^{3}$ | $56.9751\times10^{6}$ | $53.6313\times10^{6}$ |
| Soil | $53.6063\times10^{3}$ | $41.8249\times10^{6}$ | $38.8446\times10^{6}$ |
| IRON | $610.53\times10^{3}$ | $211.246\times10^{6}$ | $194.88\times10^{6}$ |
| COPPER | $842.936\times10^{3}$ | $251.576\times10^{6}$ | $235.226\times10^{6}$ |
| CARBON | $44.4118\times10^{3}$ | $50.1457\times10^{6}$ | $47.521\times10^{6}$ |
| WATER | $24.7508\times10^{3}$ | $23.3091\times10^{6}$ | $21.9412\times10^{6}$ |
| ALUMINUM | $78.0999\times10^{3}$ | $56.5935\times10^{6}$ | $53.6313\times10^{6}$ |
| TITANIUM | $219.835\times10^{3}$ | $99.522\times10^{6}$ | $94.3129\times10^{6}$ |

*Table 2: Production cuts in eV*

Only the disrupted beam, beamstrahlung and coherent pairs were used in the simulation, as the power contribution from the Bhabhas and incoherent pairs is significantly smaller. The output files from GUINEA-PIG were loaded into FLUKA using a customised `SOURCE` routine. A range of collision offsets were used, from -30 to 30 nm vertically and from -200 to 200 nm horizontally.

Cartesian `USRBIN` commands were used to measure energy deposition across the whole system. The `SCORE` command was used to record the energy deposited in each element. Also the passage of all particles crossing several planes in *z* was record, so that counts at potential detectors could be made.

## 3.4. ENERGY DEPOSITION

The magnets in the PCL must be protected from the disrupted beam and collision products, to avoid heating and radiation damage. While the core of the disrupted beam, which contains most of the power, can be transported all the way to the final dump, there are many particles with lower energies or angular divergence that would hit the magnets or beam pipe. Between the first 5 magnets that make up the first bend, there are 4 iron masks. These collimate the low energy particles that receive strong bends in the magnets.

The intermediate dump is designed to remove all the opposite sign particles, and the same sign particles with energy less than 83 % of the collision energy.

Table 3 shows the power absorbed at each of the dumps, masks and magnets for the disrupted beam and the collision products. It can be seen that the masks absorb several kW of power before the intermediate dump, while the window magnets receive less than 100 W each. The losses in the C magnets are similarly below 100 W each, although there are losses of the order of kilowatts in the beam pipe wall around the C magnets.

| | Disrupted beam | Photons | Co + | Co - |
|---|---|---|---|---|
| Main Dump | 9.97 M | 3.61 M | 98.38 K | 94.67 |
| Int Dump | 56.87 K | 108.44 | 19.27 K | 124.60 K |
| Mask 1 | 16.92 | 2.01 | 3.42 | 78.56 |
| Mask 2 | 193.30 | 0.01 | 132.34 | 412.90 |
| Mask 3 | 1.10 K | 0.00 | 826.16 | 602.65 |
| Mask 4 | 2.99 K | 0.00 | 1.65 K | 1.52 K |
| W Mag 1a | 0.00 | 0.00 | 0.00 | 0.00 |
| W Mag 1b | 0.00 | 0.00 | 0.00 | 0.00 |
| W Mag 2 | 8.34 | 0.00 | 7.33 | 6.88 |
| W Mag 3 | 26.62 | 0.02 | 11.83 | 90.81 |
| W Mag 4 | 43.05 | 0.00 | 24.42 | 22.81 |
| C Mag 1 | 39.38 | 2.43 | 7.39 | 47.44 |
| C Mag 2 | 10.96 | 1.80 | 2.30 | 7.89 |
| C Mag 3 | 63.04 | 0.24 | 16.59 | 1.75 |
| C Mag 4 | 48.55 | 0.01 | 12.70 | 0.38 |

*Table 3: Beam loss at elements, in Watts*

Figures 7 and 8 show the energy deposition along the PCL from the top and side. The losses in the main and intermediate dumps are clearly visible, the masks, magnets, beam pipe and tunnel walls can also be seen. Figure 9 shows a more detailed view of the bend sections and the intermediate dump.

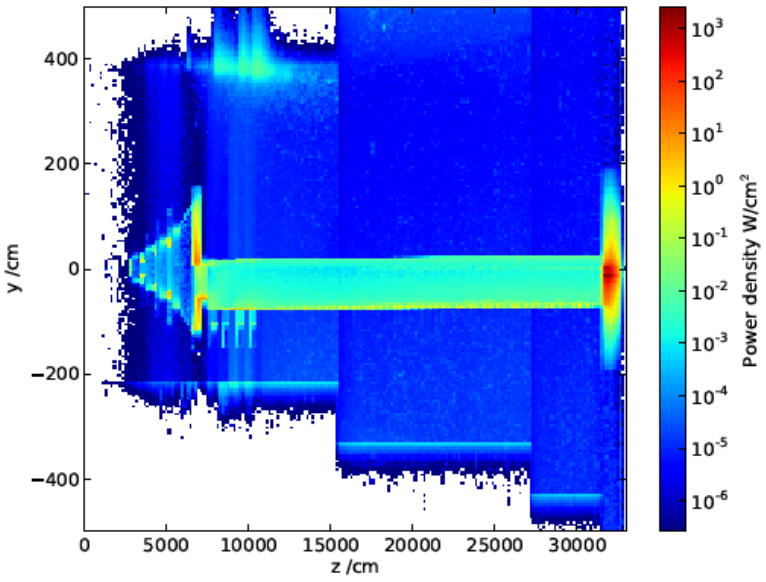


*Figure 7: Energy deposition in PCL from side*

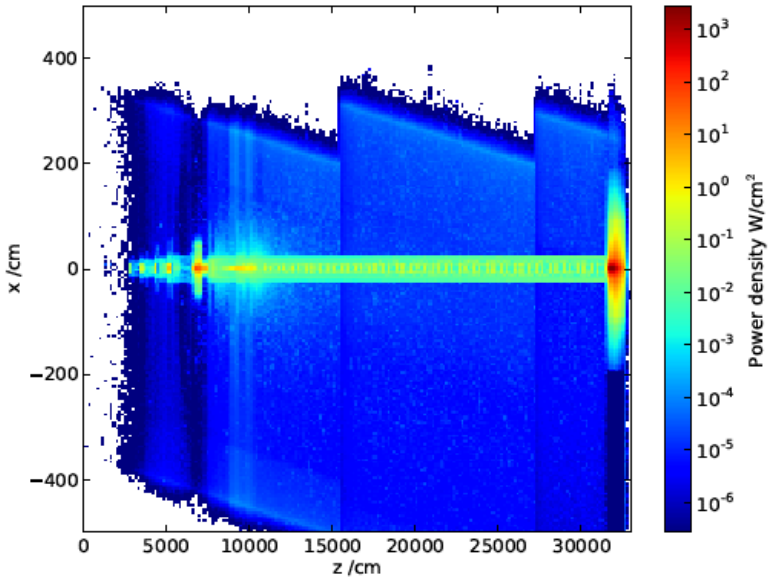


*Figure 8: Energy deposition in PCL from above.*

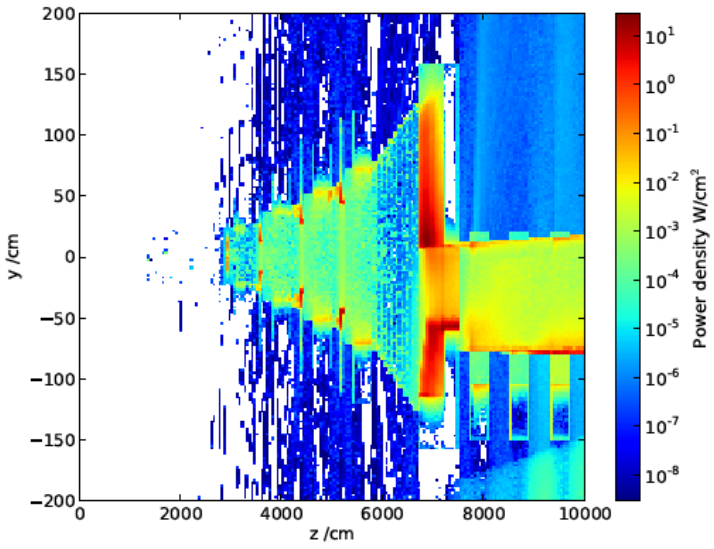


*Figure 9: Energy deposition in first 100 m of the PCL from side.*

Around 98 % of the power from the collision reaches the main dump. In the zero offset collision case it is spread across the full height of the 60 cm dump entrance window.

The power density on the plane just before the entrance window is show in figure 10, there are distinct peaks from the beamstrahlung and disrupted beam. Figure 11 shows the energy deposition within the main dump.

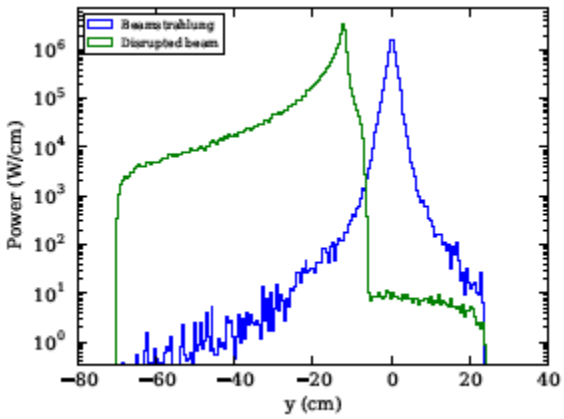


*Figure 10: Power density of disrupted beam and beamstrahlung reaching the main dump.*

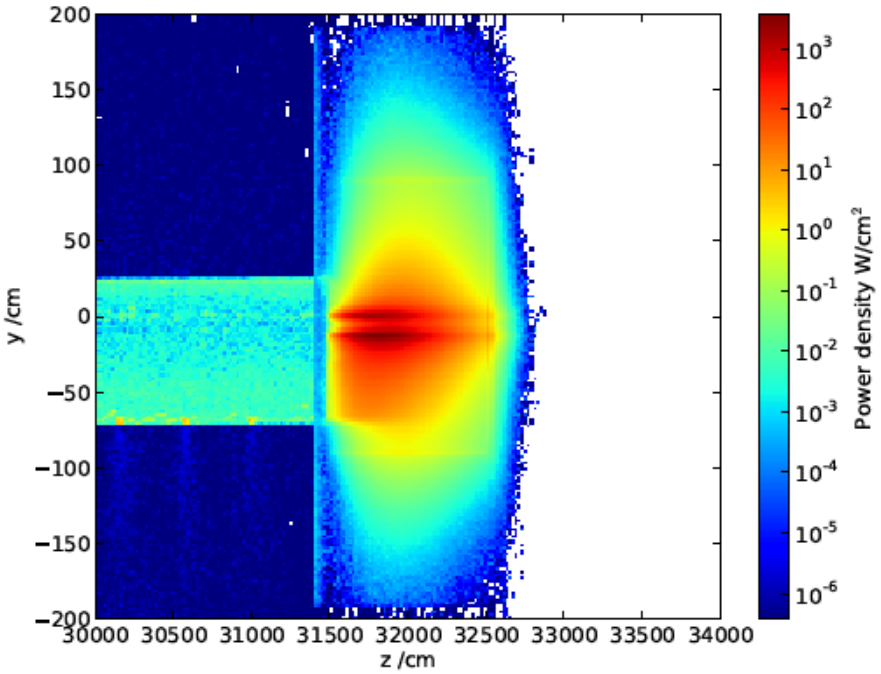


*Figure 11: Energy deposition in first main beam dump.*

These figures are similar to previous modelling performed with BDSIM [6] and GEANT4 [7,8] on the older versions of the geometry [3].

## 3.5. SIGNAL AT DETECTORS

The cone of beamstrahlung photons carries a lot of information about the collision, so it is desirable to place photon detectors in the PCL to measure it. In a head on collision there is 3.6 MW of power in the photon cone, so any detector must be placed in the edge of its distribution. The detector must also not be placed in the path of the disrupted beam, or where it will see too much background from the other collision products. There is not enough signal out side of the beam pipe, for a detector, so it must be inside the vacuum.

Initially beamstrahlung photons have a similar path to the disrupted beam and other products. The must be magnetically separated from the charged particles in the first bend, same sign particles downwards and the opposite sign particles upwards. After the intermediate dump which removes the opposite sign particles there is a separation between the center's of photon cone and the disrupted beam of around 10 cm, as shown in figure 12. This provides some space to locate the detectors.

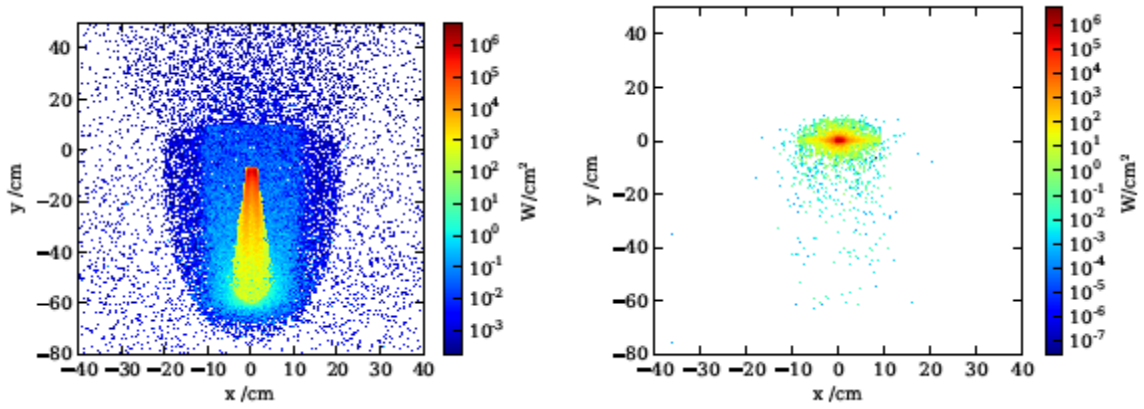


*Figure 12: Disrupted beam (left) and beamstrahlung photons (right) after the intermediate dump at 76m from the IP.*

If a photon counter is placed at 109 m from the IP, after the second bend and 10 cm above reference line of the centre of the photon cone at zero offset, the signal has a clear dependence on the collision offsets as shown in figure 14. The background is the sum of all other sources of particles reaching the detector, it may not be detrimental to the determination of the signal. For horizontal offsets the signal is a sharp peak with sigma of 46.3 nm. Assuming that the detector response is linear to energy flux, to detect a 10% drop in luminosity the detector would need to be sensitive to a 15% drop in signal. This enhancement is due to offsets causing a drop in photon count and also a deflection of the photon cone away from the detector.

The dependence for vertical offsets does not peak centrally as the power of the beamstrahlung has a local dip for zero offset as seen in earlier section. Fitting from -10 to 10 nm dip has sigma of around 8 nm, and so a 1.3 nm offset produces around 0.1% change in the signal compared to the peak. It is not symmetrical as for negative vertical collision offsets the photon

cone is deflected upwards. A symmetrical response could be achieved by placing a second detector at the bottom of the photon cone, however this position would put it in the very high power of the disrupted beam. The peak at 2.5x10$^{9}$ GeV per crossing is equivalent to 6.2 kW over the 10x10 cm detector.

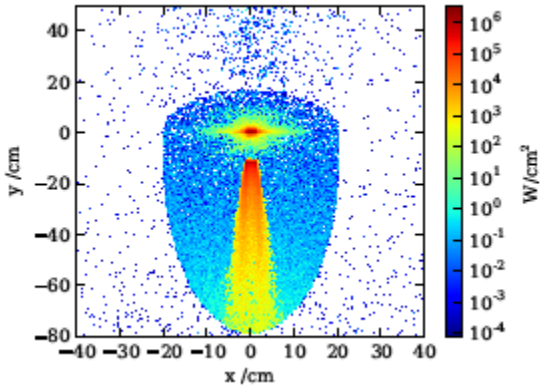


*Figure 13: Flux at 109 m from the IP from all sources.*

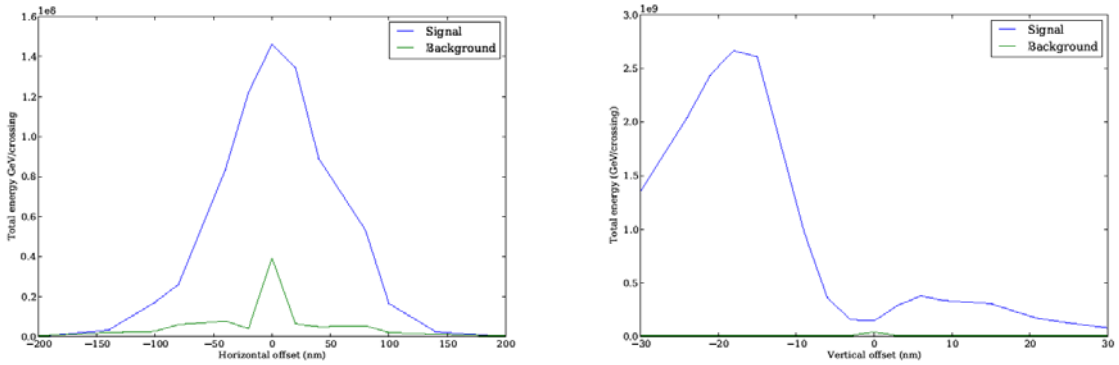


*Figure 14: Signal from beamstrahlung photons, and background from other products at 10 cm detector at y=10 cm at 109 m from the IP for horizontal (left) and vertical collision offsets (right).*

Another possible location for detectors is at the side of the beam pipe, to sample the edge or the wide photon cone. By using two or more detectors above and below the mean height of the photon cone, vertical deflections from vertical collision offsets are measurable. A range of 4x4 cm detectors were simulated offset from the center of the photon cone by 10 cm in *x*. Figure 15 shows two schemes, a two detector version with detectors positioned at 2 cm above and below the *y*=0 line, and 3 detector scheme with an additional detector in the middle.

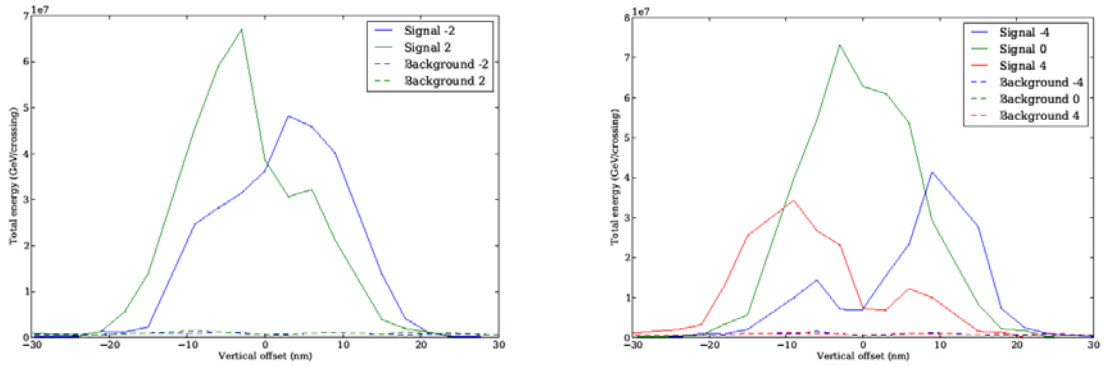


*Figure 15: Signal from beamstrahlung photons, and background from other products at 4 cm detectors positioned 10 cm to the side of the photon cone, with 2 detector (left) and 3 detector (right) scheme.*

The signals from multiple detectors could be combined, to give sum and difference values. Figure 16 shows the sum and difference for the two detector scheme, and various possible sums for the three detector scheme. In order to optimise the luminosity the beams could be coarsely aligned by maximising the sum signal, and then fine tuned by zeroing the difference signal. Fitting a straight line to the difference signal between -10 to 10 nm, gives a signal change of around 6% and 5% of the full signal range for the 2 detector and 3 detector schemes, for vertical beam offsets of 1.3 nm.

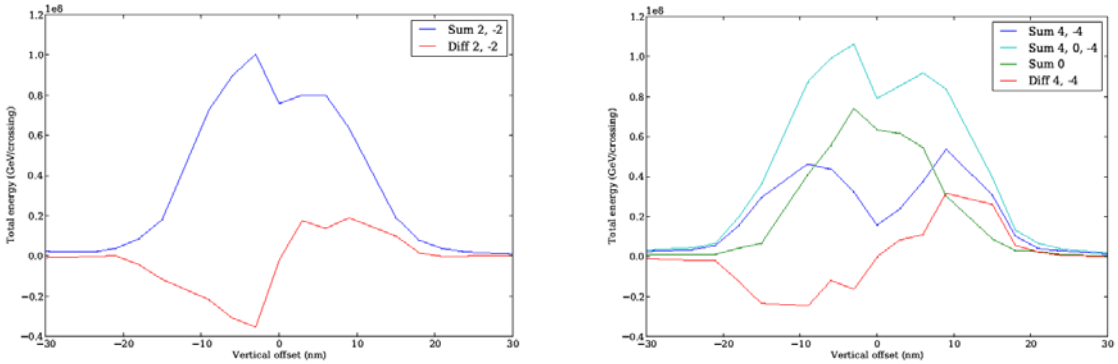


*Figure 16: Combined signals at 4 cm detectors positioned 10 cm to the side of the photon cone, with 2 detector (left) and 3 detector (right) scheme.*

## 3.6. CONCLUSION

The luminosity of collisions at the CLIC IP depends strongly on beam alignment, especially in the vertical direction. The collisions create large numbers of beamstrahlung photons as well as other products. The distribution and intensity of the photons depends on the collision offsets. By detecting the edges of the photon distributions with multiple detectors it is possible to measure the collision offset and correct the alignment of the beam in order to maximise luminosity.

These initial studies suggest that with a single detector above the beam an horizontal offset causing 10 % luminosity drop would give a 15% change in signal, however to detect equivalent vertical offset it would have to measure signal changes down to around 0.1%. By adding a set of 2 or 3 detectors at the side of the beam, vertical offset causing a 10% luminosity drop can be detected by 5% changes in signal. Simulations with greater offset resolution and a detailed detector response would be needed to confirm this.

## 3.7. APPENDIX

### 3.7.1. PCL layout

Table 4 shows the locations and dimensions of the magnets, masks and beam pipe from the IP to the face of the ID. The meaning of the dimensions are shown in figure 17. The masks have the same shape, but no magnet coils. The beam pipe sections only have *c* and *d* dimensions.

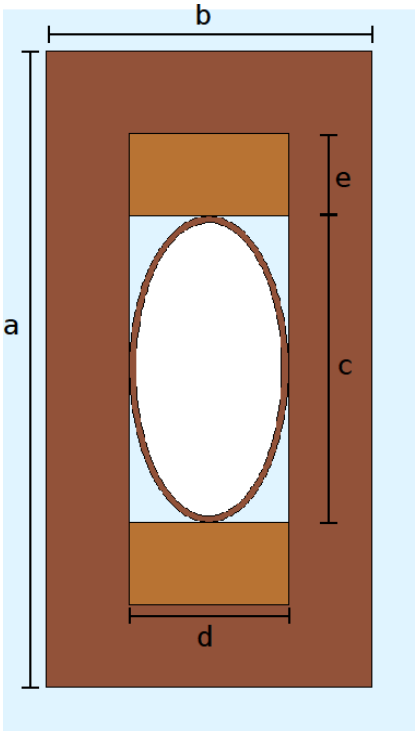


*Figure 17: Window magnet dimensions.*

| **Component**/beampipe | $a$ [mm] | $b$ [mm] | $c$ [mm] | $d$ [mm] | $e$ [mm] | $s$ [m] |
|---|---|---|---|---|---|---|
| IPtoM1 | - | - | 440 | 200 | - | 0 |
| **Mag 1A** | 976 | 494 | 450 | 222 | 127 | 27.5 |
| M1AtoCOLL1A1B | - | - | 440 | 200 | - | 28 |
| **Coll 1a-1b** | 1000 | 500 | 200 | 132 | - | 29 |
| COLL1A1BtoM1B | - | - | 440 | 200 | - | 29.5 |
| **Mag 1B** | 976 | 494 | 450 | 222 | 127 | 30.5 |
| M1BtoCOLL12a | - | - | 522 | 222 | - | 34 |
| M1BtoCOLL12b | - | - | 542 | 227 | - | 35.25 |
| **Coll 1-2** | 1542 | 771.25 | 256 | 308.5 | - | 35.55 |
| COLL12toM2a | - | - | 620 | 248 | - | 36.45 |
| COLL12toM2b | - | - | 702 | 270 | - | 36.75 |
| **Mag 2** | 1362 | 692 | 712 | 296 | 127 | 38 |
| M2toCOLL23a | - | - | 801 | 292 | - | 42 |
| M2toCOLL23b | - | - | 825 | 297 | - | 43.25 |
| **Coll 2-3** | 1892 | 946.25 | 570 | 378.5 | - | 43.55 |
| COLL23toM3a | - | - | 921 | 318 | - | 44.45 |
| COLL23toM3b | - | - | 1020 | 340 | - | 44.75 |
| **Mag 3** | 1828 | 914 | 1030 | 370 | 127 | 46 |
| M3toCOLL34a | - | - | 1137 | 362 | - | 50 |
| M3toCOLL34b | - | - | 1165 | 367 | - | 51.25 |
| **Coll 3-4** | 2242.5 | 1121.2 | 900 | 444 | - | 51.55 |
| COLL34toM4a | - | - | 1277 | 388 | - | 52.45 |
| COLL34tom4b | - | - | 1394 | 410 | - | 52.75 |
| **Mag 4** | 2378 | 1164 | 1404 | 444 | 127 | 54 |
| M4toINTDMPa | - | - | 1517 | 424 | - | 58 |
| M4toINTDMPb | - | - | 1640 | 439 | - | 59 |
| M4toINTDMPc | - | - | 1763 | 453 | - | 60 |
| M4toINTDMPd | - | - | 1886 | 468 | - | 61 |
| M4toINTDMPe | - | - | 2008 | 482 | - | 62 |
| M4toINTDMPf | - | - | 2131 | 497 | - | 63 |
| M4toINTDMPg | - | - | 2254 | 511 | - | 64 |
| M4toINTDMPh | - | - | 2377 | 526 | - | 65 |
| M4toINTDMPi | - | - | 2500 | 540 | - | 66 |
| Int. dump start | - | - | - | - | - | 67 |

*Table 4: Window shape magnets and collimators locations and dimensions. s is the location of the upstream face of the component.*

Figures 18 and 19 show the intermediate dump, it is 8 m long, and split into several sections. The frame of the ID is composed of iron, inside there are graphite absorbers and water for cooling. The top and bottom of the water tanks have 20 mm aluminium layers. The last 3.2 m have no graphite or water. From the start of the ID onwards the beam pipe has a shape composed of 2 half ellipses as shown in figure 20, to better accommodate the distribution of the beamstrahlung and disrupted beam.

Table 5 shows the dimensions of the aperture though the ID.

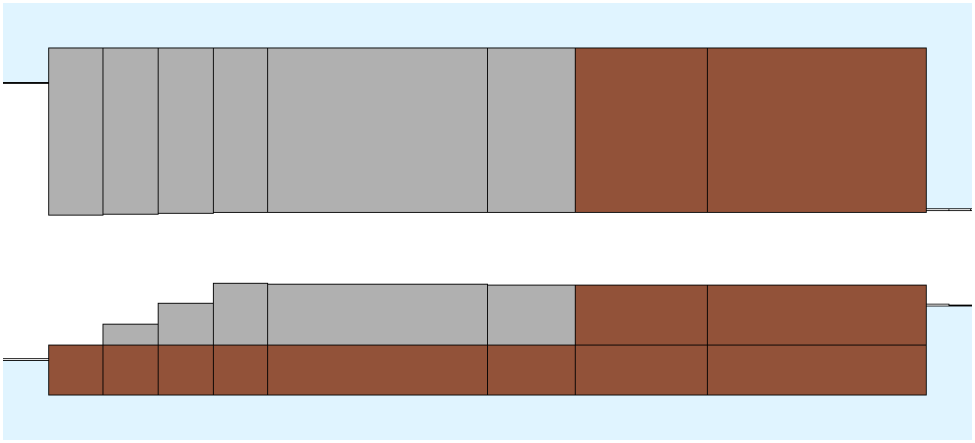

*Figure 18: Intermediate dump side.*

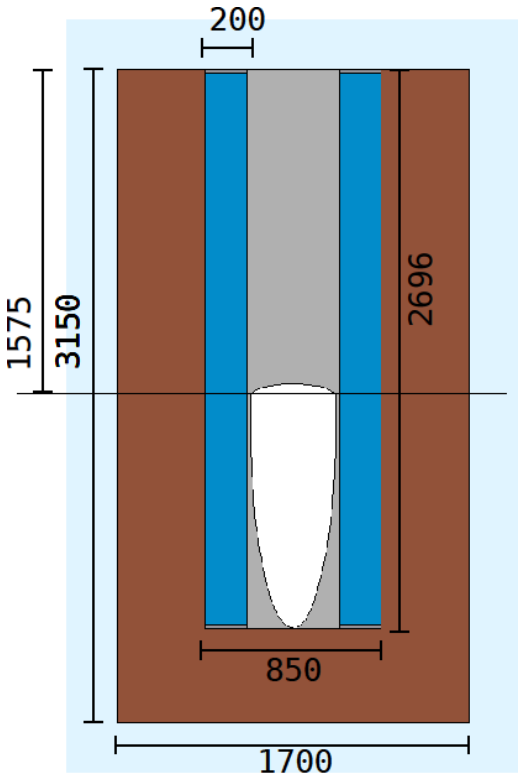


*Figure 19: Intermediate dump along beam axis.*

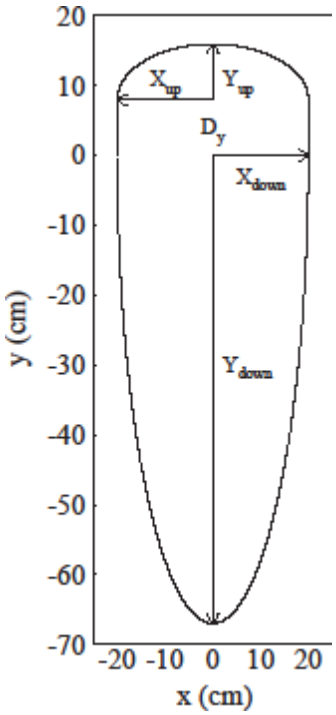


*Figure 20: Shape of beam pipe from ID onwards.*

| Section | $l$ [m] | $X$ [mm] | $Y_{\text{up}}$ [mm] | $Y_{\text{down}}$ [mm] | $D_y$ [mm] |
|---|---|---|---|---|---|
| 1 | 0.5 | 206 | 57.5 | 1000 | 120.96 |
| 2 | 0.5 | 180 | 65 | 810* | 123.52 |
| 3 | 0.5 | 135 | 72.5 | 620 | 126.08 |
| 4 | 0.5 | 90 | 80 | 430 | 128.64 |
| 5 | 2 | 90 | 80 | 430 | 138.88 |
| 6 | 0.8 | 90 | 80 | 430 | 149.12 |
| 7 | 1.2 | 90 | 80 | 430 | 149.12 |
| 8 | 2.0 | 90 | 80 | 430 | 149.12 |

*Table 5: Intermediate dump aperture parameters.*

After the main dump there are four C-shaped 1 T dipole magnets that bend the beam back to horizontal. They are each 4 m long and of the dimensions in figure 21. They are positioned at 77, 85, 93 and 101 m from the IP.

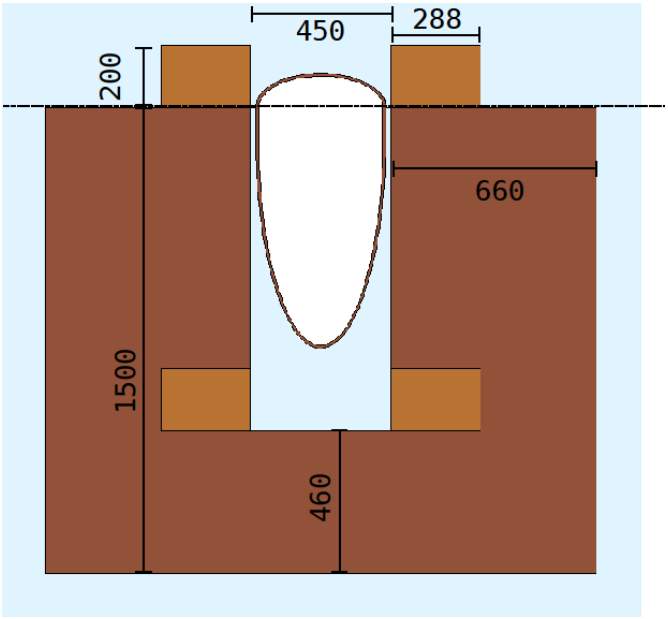


*Figure 21: C shaped magnet.*

From the ID to the end of the C magnets, the beam pipe varies in size, with the parameters give in table 6. Between the end of the last C magnet and the main dump the beam pipe shape changes continuously to form a race track shape - $D_y$=54 cm, $Y_{up}$=$Y_{down}$=20 cm - vertically displaced by -4 cm. This transformation takes place in 50 steps, each 4.18 m long, ending 1 m before the face of the dump, where the dump concrete shielding begins.

| $s$ [m] | $l_{\text{step}}$ [m] | $N_{\text{steps}}$ | $(Y_{\text{up}})\Delta Y_{\text{up}}$ [cm] | $(D_y)\Delta D_y$ [cm] |
|---|---|---|---|---|
| 75 | 0.2 | 10 | (10) 0 | (8) 0.075 |
| 77 | 4.0 | 1 | (10) 0 | (9.0) 0 |
| 81 | 0.2 | 10 | (11) 0.1 | (9.2) 0.03 |
| 83 | 0.2 | 10 | (12) 0 | (9.5) 0.025 |
| 85 | 4.0 | 1 | (13) 0 | (10.2) 0 |
| 89 | 0.2 | 5 | (14) 0 | (10.25) 0.05 |
| 90 | 0.2 | 15 | (14) 0 | (10.5) 0.0167 |
| 93 | 4.0 | 1 | (15) 0 | (11.00) 0 |
| 97 | 0.2* | 20 | (16) 0 | (11.00) 0.01 |
| 101 | 4.0 | 1 | (16) 0 | (11.2) 0 |

*Table 6: Beam pipe dimensions from the end of the intermediate dump at s=75 m to the end of magnet 8 at s=100 m. The table shows s of the beginning of first step. The next two columns give the step length and number of steps. The following columns give the beam pipe dimensions. The bracketed numbers are the value at s. The numbers outside the brackets are the corresponding step sizes. X=20 cm and $Y_{down}$=67.5 cm are constant.*

The main dump is a water tank with radius 0.9 m and length 10 m, with its front face 315 m from the IP. Around this is a 2 cm titanium jacket and a 1 m layer of concrete. There is an additional 4 m concrete wall behind the dump. The window to the dump is a 15 mm layer of carbon, followed by 2 mm of aluminium.

# 4. INTERNATIONAL LINEAR COLLIDER BEAM DELIVERY SYSTEM DESIGN

## 4.1 CHANGES TO ILC BDS DESIGN

The Strawman Baseline 2009 proposal [9] from the ILC Project Management Design Team proposes major changes to the published Reference Design Report (RDR) baseline [10] to address both a reduction in cost and a more complete and robust design approach, taking into consideration the ongoing R&D plans. One of the items for consideration in this proposal is the central integration of several RDR systems into a central common location. The motivation for this change is the simplification of the central region tunnelling and civil engineering.

The central integration includes the sources in the same tunnel as the BDS. Relocation of the positron production system to the downstream end of the electron linac means placing it just before the beginning of the electron BDS. These changes need suitable design modifications to the layout of this area including modifications to the machine protection and fast abort lines, as well as a dogleg design to provide the required transverse offset for the positron target. In addition to providing the required transverse offset, the emittance growth due to incoherent synchrotron radiation at 500 GeV beam energy (1 TeV centre of mass (CM)) in the design needs to be below a few percent. Similar to the RDR design, the BDS design remains compatible with a 1 TeV CM upgrade which is expected to be accomplished by installing additional dipoles and replacing the final doublet, and thus the dogleg design needs to be designed to deal with emittance growth at all possible beam energies. The proposed design [11] meets all the constraints and has been accepted for the Technical Design Phase of the ILC.

## 4.1. LAYOUT AND DESIGN CONSIDERATIONS

The most notable feature of the new electron BDS layout is the introduction of the dogleg to create the required transverse offset between the electron beamline and the positron photon target. Another important consideration is the protection of the undulator from miss-steering, as well as an electron beam with significant energy errors, and which now shares the same systems foreseen for the BDS. These changes apply only to the electron side.

The RDR has sacrificial collimators in the beginning of the BDS to protect it from any beam with errors entering from the large aperture of the main linac (r = 70 mm) into the small aperture (r = 10 mm) of the BDS. In the new layout, the small aperture undulator (~8 mm full) is located immediately after the linac and thus it needs to be protected against any error beam from the linac. This is achieved by moving the sacrificial collimator section, and an energy chicane to detect the off energy beam, in front of the undulator as shown in Fig. 22. Any beam entering this section with errors will be detected and sent to the fast abort line, before entering, and possibly damaging, the undulator. The fast abort line is presently the same length as the RDR abort line, which was designed as both a fast abort line as well as a tuning line (the positron BDS side still has this combined functionality). However, the fast abort beam dump needs to be able to take only the number of bunches between the abort signal and stopping the beam at the extraction of the damping ring, and does not need to be a full power beam dump.

The matching line to the undulator needs to allow sufficient transverse separation for the abort line and then matching into the undulator FODO cell. The photons generated in the undulator will pass through a drift of 400 m to the positron target. To implement the positron target, and the remote handling of the components in this area, a transverse offset of 1.5 m is required between the electron beamline and the photon target. The remote handing area needs a drift space of approximately 40 m in length where no BDS components are placed. This is achieved by using a matching section after the undulator to match into a dogleg, the dogleg itself giving a transverse offset of 1.5 m with a 40 m long drift section at the end.

The 40 m long drift is followed by a matching section into the skew and coupling correction section, a chicane for detection of laser wire photons and a slow tune-up (DC tuning) line leading to a full power beam dump. Since the fast abort functionality is being taken care of by the fast abort line before the undulator, the energy acceptance of the DC tuning line is much reduced and thus the DC tuning line can be shortened using only DC magnets. The polarimeter chicane will be located just after the take-off section for the tuning line, which is not shown in the layout. The betatron and energy collimation, energy spectrometer and final focus sections remain similar to the RDR.

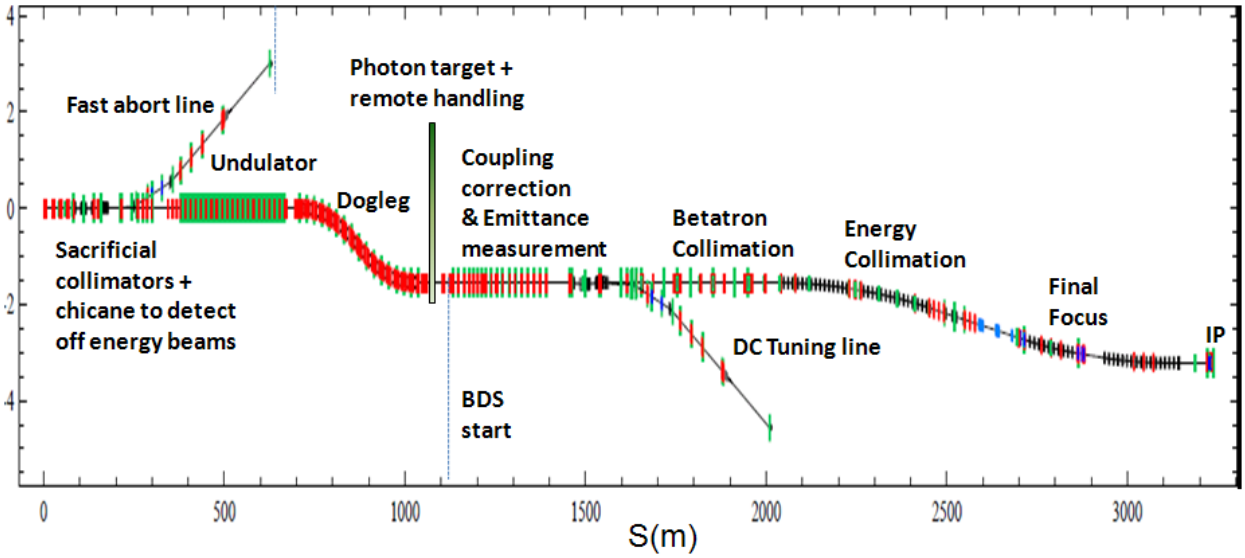


Figure 22: Layout of electron side beam delivery system, IP is the interaction point

### 4.1.1. Dogleg Design

The dogleg lattice has been designed as a TME (Theoretical Minimum Emittance) lattice. This keeps the emittance growth due to synchrotron radiation at 1 TeV CM to be within a few percent. The dogleg provides an offset of 1.5 m in 400 m as required and the emittance growth at 1 TeV CM is ~3.8%. The dipoles in the dogleg are presently not decimated as in the rest of the RDR BDS, but can be for better tuning performance at 500 GeV CM. The dogleg lattice design is severely constrained due to the available space of 400 m longitudinally, and with a minimum 1.5 m transverse offset. The requirements on allowable emittance growth constrain the dipole bend angles available to ~1.1 mrad, which in turn lead to constraints on the required focusing through the dipoles. The limited space also constrains the room available

for magnets outside of the dipoles. Together, this leads to a very compact, strong focusing lattice. To explore the solution space in terms of quadrupole magnet design, 3 lattice solutions were considered with different maximum pole-tip fields. The three designs all feature 2 quadrupole families per cell, with one central dipole. In the first half of the dogleg, the dipoles bend away (+bend), and in the second half towards (-bend) the BDS. The first and last dipoles in each of the two bending sections have lower bend angles to match the dispersion into, and out of, the dogleg. These dipoles can be used to match and correct incoming errors to minimise the emittance growth seen in the dogleg section.

### 4.1.2. Tuning and Tolerances

Due to the space constraints and strong focusing in the dogleg design, it is expected that the tolerances will be tight. The results of uncorrected mismatch entering the lattice are given in Table 7, for a 10% emittance growth in the lattice at 1TeV CM (cf. 3.8% nominal).

Table 7: Tolerances for the 80Tm dogleg design

| Parameter | Tolerance | With Correction |
|---|---|---|
| Initial $\alpha_x$ | -1.7 – 1.71 | N/A |
| Initial $\beta_x$ (m) | $10 \rightarrow 200$ | N/A |
| Initial $\eta_x$ (mm) | -9.5 – 11 | -21 – 27 |
| Initial $\eta_x$' (mrad) | -0.13 – 0.2 | -0.32 – 0.4 |
| Initial x (mm) (centroid) | -0.13 – 0.21 | -0.6 – 0.75 |
| Initial x' (μrad) (centroid) | -2 – 3.2 | -11.5 – 12.9 |

The tight tolerances shown in Table 7 arise due to the strong focusing nature of the dogleg-design, itself dictated both by space constraints as well as the requirement to minimise the emittance growth in the dogleg. As the dispersion function drives the emittance growth, it is clear that the lattice presents a tight constraint on the allowable incoming dispersion function miss-match. As has been noted, this miss-match can be partially corrected by using the 4 "end" dipoles (2 +bend, 2 –bend) to correct the incoming, and outgoing, dispersion, whilst also minimising the subsequent emittance growth. A further constraint is to minimise the outgoing trajectory error, as this would feed in to downstream elements of the BDS. This trajectory error can also be corrected downstream of the dogleg if required. The improvement on the incoming dispersion tolerances, due to correction using the 4 "end"-dipoles, is illustrated in Fig. 23, showing an approximate factor of 2 improvement at 10% emittance growth.

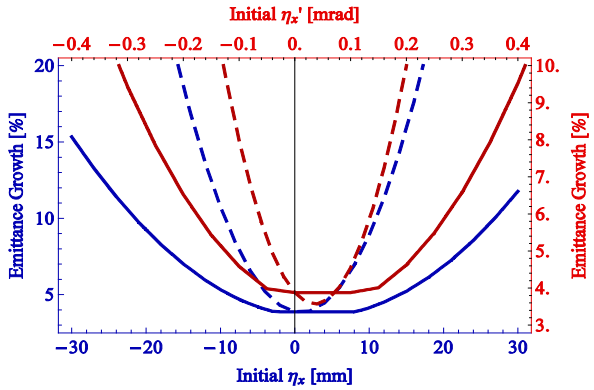


Figure 23: Emittance growth due to incoming dispersion errors, with (solid) and without correction (dashed)

### 4.2. LATTICE REPOSITORY

A note was published [12] to summarise the status of changes made to ILC BDS decks after ILC RDR was published and comments on the remaining lattice design work which needs to be done in the future.

### 4.3. CONCLUSIONS

The TME dogleg design satisfies the layout constraints and gives ~4% emittance growth at 1 TeV CM energy. Due to the strong focussing required in this lattice, the implications on tuning and tolerances have been presented, showing very tight tolerances on the incoming dispersion, as well as the required trajectory correction. Correction of these errors using the 4 “end” dipoles in the design has shown that it is possible to widen the tolerance levels significantly. However, additional correction for the trajectory within the dogleg needs to be looked at further and to understand if decimation of dipoles will be useful to relax the tolerances at 500 GeV CM.

## 5. ATF2 TUNING PROCEDURES AND TESTS

### 5.1. ATF2 GOALS

ATF2 is a test facility with the aim of proving the concept of local chromaticity correction Final Focus System (FFS) design proposed in [13]. An important technical challenge of ILC and CLIC is the collision of extremely small beams of a few nanometers in size. This challenge has three distinct issues: creating small emittance beams, preserving the emittance during acceleration and transport, focusing the beams to nanometers and colliding them. Accelerator Test Facility (ATF) [14] at KEK was built to create small emittance beams, and has succeeded in obtaining an emittance that almost satisfies the ILC requirements. The ATF2 facility [15], which uses the beam extracted from ATF damping ring, was constructed to address two major challenges of ILC: focusing the beams to nanometer scale using an ILC-like final focus and providing nanometer stability.

The two ATF2 goals, first one being achievement of ~35nm beam size, and second being achievement of nanometer scale beam stability at IP. Whilst addressing these two major challenges, the facility will address some open questions such as tuning difficulty, impact of the known magnetic errors and the compatibility of the Shintake monitor with a probably enlarged halo, which will benefit to achieve challenging goals of future linear collider.

## 5.2. ATF2 ORBIT CORRECTION AND TUNING PROCEDURES

### 5.2.1. Orbit Correction

Orbit correction is an important part of the operation of an accelerator. The machine was designed with magnets and instruments where the beam passes through the exact centre of all the components unless the path of the beam is being altered. When the beam passes off-centre through the magnets it is affected by the magnets' multipole fields. These fields cause alterations to the path of the beam and the parameters of the beam, including beamsize growth. Orbit correction techniques for the ATF2 extraction line and final focus were developed and compared in simulations and real world tests with alternative techniques.

Of the several methods of orbit correction that were investigated for use on ATF2 a method known as 'modular global orbit correction' was found to give the best results in simulation tests. The modular global orbit correction method treats the extraction and final focus regions as separate sections and corrects the orbit of each one in turn. This method was adapted into a working orbit correction program for use on ATF2. The modular global orbit correction method was tested and compared in simulations and real world tests with a method developed by another team. The modular global orbit correction method was shown to be significantly faster than the alternative method while offering comparatively similar results. Both methods were shown to suffer from 50 - 100% over-correction in the final focus section. This was found to be a result of an intensity dependence with the stripline BPMs.

The extraction line orbit correction algorithm is used first and then followed by the final focus orbit correction algorithm. The ATF2 was simulated with a full set of errors and each optimised orbit correction algorithm was applied for 100 iterations. The horizontal and vertical orbits of ATF2 have both been significantly corrected (in simulations) as shown in Fig.24.

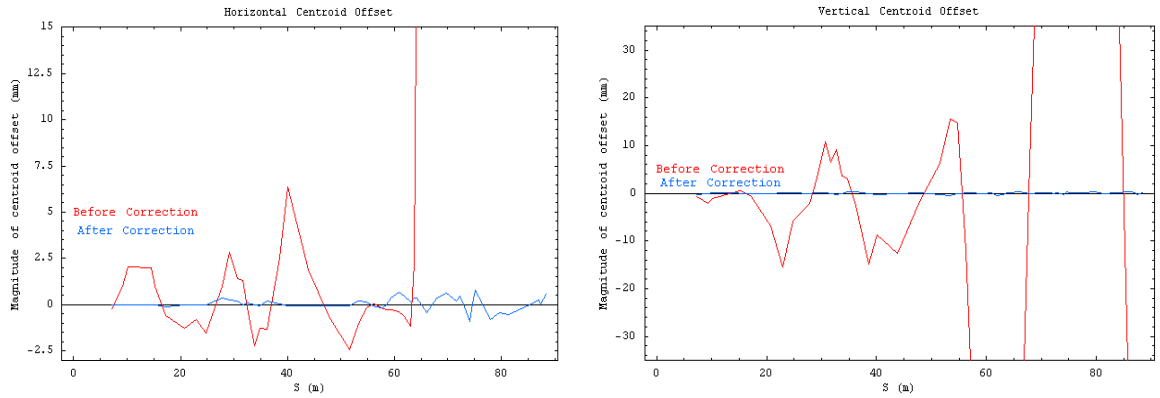


Fig 24: The horizontal (Left) and Vertical (Right) ATF2 orbit before and after 100 iterations of optimised extraction line orbit correction and 100 iterations of optimised final focus orbit correction have been applied.

### 5.2.2. Tuning Procedures

In order to reach a goal of achieving ~35 nm beam spot size at the IP, one of the required tools is a set of 'tuning knob' algorithms that will autonomously optimise the parameters of a set of five sextupoles within the 'final focus' of ATF2. The variable parameters of the sextupoles are the horizontal and vertical position, along with the roll angle and sextupole strength of each sextupole magnet. Traditional methods for the development of the sextupole-based tuning knobs have been developed [16], along with a novel approach. The novel sextupole-based tuning knob method known as the 'rotation matrix' method has been developed [17]. The traditional method uses the Twiss parameters and the average position and angle of the particles of the beam, whereas the rotation matrix method uses the 6-dimensional coordinates of the beam. The traditional method can be thought of as simply morphing the beam with errors into the desired beam and the rotation matrix method can be thought of as compressing and rotating the beam with errors into the desired beam, as shown in Fig.25.

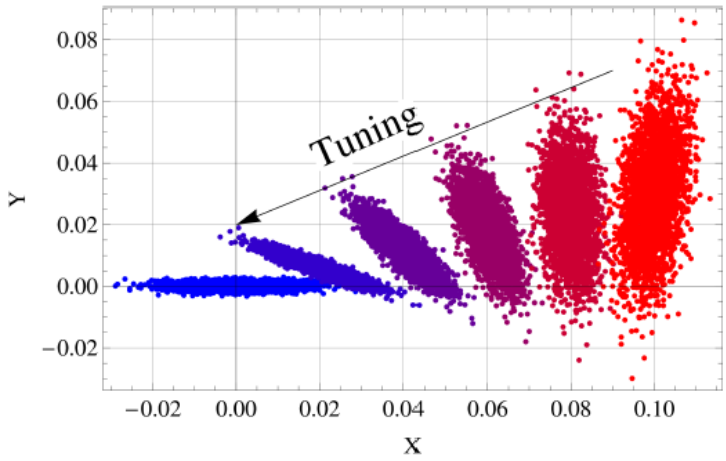


Figure 25: Beam response matrix tuning from the error beam (red) to the nominal beam (blue)

## 5.3. BEAM SPOT OPTIMISATION AT ATF2

In December 2008, construction and installation of ATF2 were completed and beam commissioning started, supported by an international team of Asian, European, and U.S. scientists. The detailed report of the status and results were presented in [18]. An extensive work on ATF2 Tuning and Alignment has been reported in the Ph.D. thesis [19].

In May 2010, the ATF2 collaboration ran its first week-long tuning session. The tuning session was designed to test the non-linear multi-knobs used to correct the vertical beam size at the IP down to the 35nm level. During the week long experiment, the trajectory, linear optics and vertical dispersion were corrected using standard multi-knobs in the EXT line of ATF2. The coupling was corrected using several dedicated skew quadrupole correctors, but due to the low repetition rate of the ATF2, the vertical emittance was corrected only down to the level of ~20pm, rather than the design 12pm. Using the final quadrupoles in the lattice it was possible to check the final focus line optics by comparing the beam size response, and correction made with upstream matching quadrupoles. The vertical beam size was measured using 10um Tungsten wires placed at the IP. With the vertical beam size after correction, at the IP, less than 1um, the sextupole multi-knobs were used to further reduce the beam size. The vertical beam size was then measured using a “Shintake-Monitor” IPBSM (Interaction Point Beam Size Monitor), which can scan the beam size accurately in different size regimes, from 20nm to ~2um, by variation of crossing angles of laser beams. The IPBSM produces accurate measurements of the vertical beam size at lower beam sizes, but can be very slow. This limits the tuning that can be performed in a given period. At the end of several iterations of the sextupole multi-knobs the vertical beam size had been reduced to less than ~300nm. However, this beam size is between 2 different operating regimes of the IPBSM, leading to reduced accuracy. This made tuning of the beam size more difficult, and it was not possible to reduce the beam size below this number. In future, a new operating regime for the IPBSM will be set-up, so as to allow a greater accuracy of measurement within this important beam-size regime. The first week long tuning session was accounted a reasonable success, with plans to perform more such sessions in the future. Although the goal of a 35nm beam size was not reached during this first attempt, lessons were learned and bugs ironed out of software.
5.4 Outcome of the EuCARD ATF2 work

- As part of the EuCARD task, the work undertaken at ATF2 to achieve ~35 nm vertical beam size covered three major problems for investigation: elimination of a source of unwanted emittance grown in the extraction region of ATF; optimisation of the orbit correction procedures in ATF2 and optimisation of the vertical beamsize tuning in the ATF2 final focus region.
- A range of orbit correction algorithms have been developed and optimised. The modular global orbit correction method has joined the selection of orbit correction software packages available on ATF2. This method is shown to be significantly faster, while offering similar results, to the alternative methods available at ATF2. The levels of dispersion along the ATF2 beam line after the orbit correction are significantly less than the starting values, which shows that the orbit correction method developed can be used to help correct other important parameters as well as the beam orbit.A novel

method “the rotation matrix method” have been developed and simulated. This method was optimised in simulations using single error simulations as well as simulations that made use of a full range of errors. In several of these simulation tests, a vertical beam size between 1 and 2 times the 35 nm goal could be achieved. However, experimentally these tests could not be performed at ATF2 due to unforeseen circumstances and it cannot be fully ruled out as a viable method for use in future application to linear collider BDS. The simulation and experimental work at ATF2 formed part of a PhD programme, and was successfully defended by the student.

- The studies on ATF2 provided an input to characterise and improve the beam orbit algorithms that may be used on the ILC BDS

The experiences gained by the EuCARD team in

- developing and testing different orbit correction algorithms
- implementing all the possible errors in real experimental set up for FFS
- developing and partially experimentally testing the tuning algorithms
- getting the experimental knowledge of scaled down FFS
- investigating issues specific to ATF2 such as off-axis beam in damping ring extraction magnets as a major cause of emittance increase
- testing experimental verification of orthogonality of tuning knobs
- understanding the limitations in achieving minimum IP spot size using different modes of Shintake IP monitor

have provided invaluable experience on the real application of these novel tuning methods, and informed the simulations for future linear colliders.

Due to a change in national policy, continued participation in the ATF2 experimental work was not continued beyond the first important experimental results, where STFC staff contributed to a week-long continuous tuning shift. The EuCARD tuning task team (STFC/UMAN) ceased experimental participation in ATF2 programme since Autumn 2010. A beam size of 300 nm was reported later [20] and recently a beam size of 65nm has been achieved at low charge [21], the major sources of multipoles in extraction line magnets and removal of the narrow aperture cavity BPMs around IPs made this significant improvement. At the time of writing this report, the international effort is progressing to achieve the final goal of ATF2 to achieve 35nm beam size. The work performed as part of the EuCARD task did, however, provided valuable input into the continuing experimental work at the facility.

Instead of work at ATF2, ILC central integration work and lattice repository was completed by the EuCARD team. Central integration was a major change to the ILC beam delivery system design from the published Reference Design Report in 2007. Additional tasks on review of CLIC beam delivery system and input to the CLIC CDR were also untaken by the team.

### 5.5 CONCLUSIONS

The ATF collaboration has completed the construction of ATF2 and started its commissioning in 2008. The facility has provided an unique experience operating the new instrumentation in real conditions and to test different orbit correction and different tuning algorithms. In the next few years, information very valuable for any future collider with local chromaticity correction and tuning of very low emittance beams can be expected.

## 6. THE ANTI-SOLENOID COMPENSATION OF THE CLIC DETECTOR SOLENOID USING IRSYN

### 6.1. ANTI-SOLENOIDS

The interaction region of CLIC is the interface between the detector and the machine and offers many beam dynamics challenges. The principle goal is the delivery of luminosity to the detector, which requires very small vertical beam sizes for the colliding beams at the interaction point (IP) and tight control over processes acting to increase the spot size. Of particular concern is the unavoidable fact that the beams in the interaction region pass through the detector solenoid, which causes luminosity degradation through a variety of mechanisms. This impact of a solenoid on the beam in the interaction region of a collider has been studied in depth in [22] and first studied for CLIC in [23]. Generally, the effect on the beam of a pure solenoid field is cancelled due to the interaction of the body and edge of the magnet, leaving an angular offset at the beam collision point. However, this cancellation is spoiled by the overlap of the solenoid with any focusing magnets, a situation which occurs at both the ILC and at CLIC. This results in residual orbit distortion and coupling aberrations in the beam distributions at the IP.

The beam traverses the solenoid at an angle (the half beam crossing angle) of 10 mrad for the CLIC interaction region, resulting in a transverse field and associated orbit deviation. The residual orbit distortion depends on the integrated field strength and the crossing angle value. The solenoid field, in conjunction with an overlap with the focusing elements, causes focusing and coupling between the transverse planes and also longitudinal coupling, or dispersive, effects. Therefore the beam is heavily distorted in all phase space planes at the IP. Furthermore the orbit deviation results in the emission of incoherent synchrotron radiation. The combination of these effects on the beam results in a rise of the vertical spot size at the IP and a reduction in machine luminosity. The compensation of these effects has been studied in depth for both the ILC and for CLIC. The preferred method is the use of anti-solenoids, which give an energy and optics independent correction. In this scheme anti-solenoids, or bucking coils, are placed over the final quadrupole QD0 to cancel the solenoid field in this region. It can be shown [22] that this cancellation of the solenoid field over QD0 restores the aberration

cancellations in the solenoid field that are broken by the presence of QD0. The SiD solenoid field has been studied for CLIC, and an anti-solenoid scheme developed [23,24] which cancels the majority of the IP beam aberrations and leaves a small amount of un-cancelled aberrations [23]. Note this scheme uses a small offset in QD0 to cancel the residual orbit at the IP and the residual aberrations can be pre-cancelled with appropriate beam delivery system tuning.

The purpose of this study, and note, is to use the code IRSYN to bench-mark the performance of the anti-solenoid compensation for the SiD solenoid for CLIC. IRSYN was a code written for the LHeC interaction region design process, to take an arbitrary field map and perform particle tracking with a Monte Carlo model of synchrotron radiation emission. Our conclusions are that the anti-solenoid as proposed for CLIC successfully compensates the majority of beam aberrations. The remaining ones can be pre-compensated in the beam delivery system. In this work we use the CLIC beam delivery system designed for a 1.5 TeV beam with an l* of 3.5m.

## 6.2. IRSYN

The code IRSYN (Interaction Region design with SYNchrotron radiation) is a code originally developed for the interaction region design for the LHeC [25,26] The code is a flexible particle tracking code, where the particle trajectories are obtained from direct integration through the magnetic fields. The magnetic layout of the interaction region is specified through a single function, which returns the magnetic field in the frame of the detector at a given spatial position. The inclusion of magnetic elements such as quadrupoles, sextupoles and solenoid field maps is possible through this universal routine. The code then tracks particles, specified from an external file or generated based on a given beam matrix, using the time reversible (hence energy conserving) Velocity-Verlet algorithm and the relativistic Lorentz force law. The effect of synchrotron radiation is included using a Monte Carlo model originally developed for LEP [27] and implemented in PLACET [28]. For a given particle step, the probability of photon emission is calculated from the radius of curvature of the particle track and its associated energy. The energy of an emitted photon is drawn from the standard incoherent synchrotron emission spectrum. The inclusion of the Monte Carlo algorithm allows the energy loss of the beam due to emission to be tracked, as well as tracking of the resulting photons through the interaction region. For further details of the code and its applications see [25,26].

## 6.3. THE CLIC SOLENOID

In this section we describe the SiD solenoid field in the CLIC interaction region, the anti-solenoid correction fields and the results of tracking the beams through this interaction region with IRSYN.

The longitudinal component of the SiD solenoid has a peak of 5 T at the interaction point. The fall-off in longitudinal distance means the field is close to zero around 9 m from the interaction point. The radial field is required to satisfy Maxwell's equations. The beam

traverses the field at an angle of 10~mrad, and so the magnetic field transverse to the particle motion (which determines the vertical force on the particles) is given by a rotation of the longitudinal and radial fields. The solenoid field extends over the last part of the final focus magnets, which start 3.5 m from the IP.

The compensation of the solenoid effects on the beam is performed with anti-solenoid coils, which surround the final quadrupole QD0 and cancel the solenoid field in this region. The anti-solenoid field configuration is described in [24] and consists of four bucking coils of radius 50 cm. The reduction of the longitudinal field around QD0 (beginning 3.5 m from the IP) is associated with an enhancement of the radial component the same region.

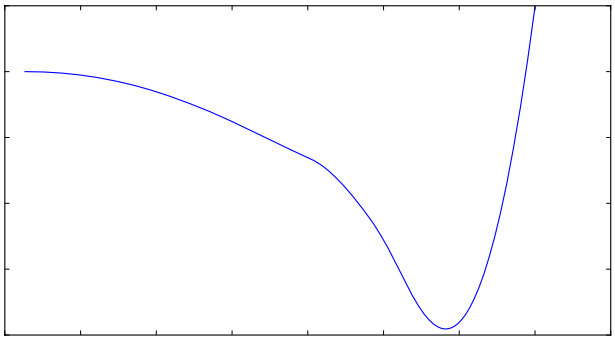

Figure 26: The vertical orbit through the solenoid with no compensation or synchrotron radiation.

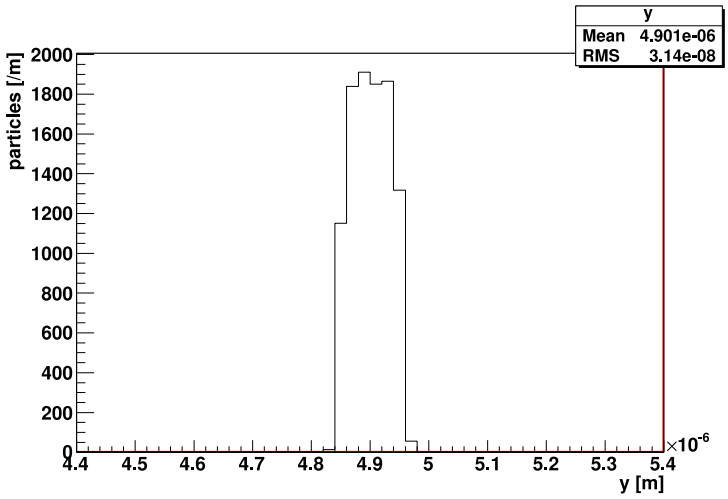


Figure 27: The vertical beam distribution at the IP for the case of an uncompensated solenoid and synchrotron radiation.

The body and edge focusing of the solenoid cancel in the presence of no other magnet elements, leaving an orbit angular offset at the IP. The presence of the final focus magnets breaks this cancellation and leads to a residual spatial offset at the IP. The resulting vertical beam orbit through the solenoid and final focus magnets, with no compensation, is shown in

figure 26 where the resulting orbit offset at the IP is 5 μm. The presence of the solenoid, and the overlap with the final focus elements, also causes cross-plane coupling at the IP, the most important of which for a small vertical spot size are the residual dispersion and x'-y coupling. The beam distributions at the IP for the case of the uncompensated solenoid, and synchrotron radiation, are shown in figures 27 and 28 The vertical spot size is shown in figure 27, which shows beam size growth and a centroid shift, and figure 28 shows the x'-y coupling and dispersion. The growth in these coupling terms due to the interaction between the solenoid and the final focus magnets is clearly seen. The impact of the synchrotron radiation on these distributions is relatively small.

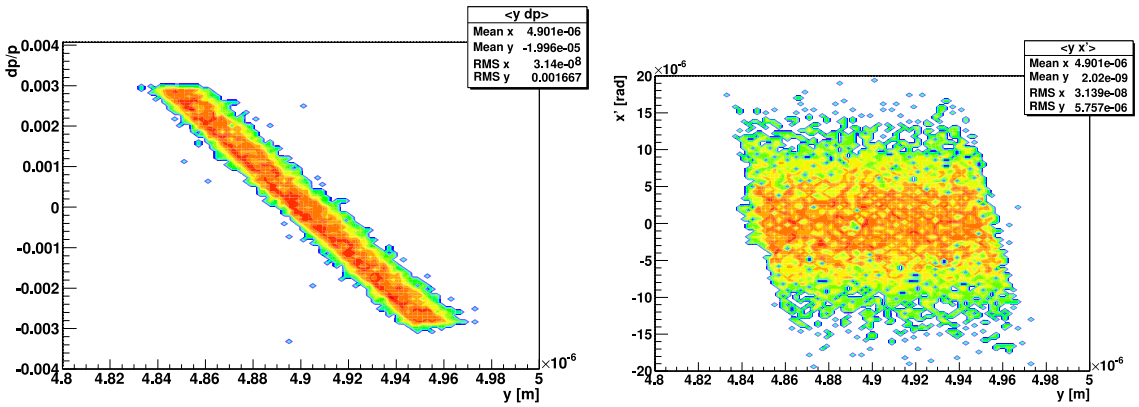


Figure 28: The vertical dispersion (left) and the x'-y coupling (right) at the IP for the case of an uncompensated solenoid and synchrotron radiation.

The corresponding plots of the beam distributions in the presence of the anti-solenoid are shown in figures 29 and 30. These distributions were obtained by tracking identical beams to the uncompensated case in the presence of synchrotron radiation through the interaction region to the IP with the inclusion of the anti-solenoid coils on QD0. Figure 29 shows the vertical beam distribution, which is corrected back to close to the nominal size. The x'-y and dispersion are shown in figure 30, showing the coupling terms are mostly, but not entirely, cancelled. We have checked the residual vertical orbit at the IP can be cancelled with a small (around 1 mum) offset of QD0.

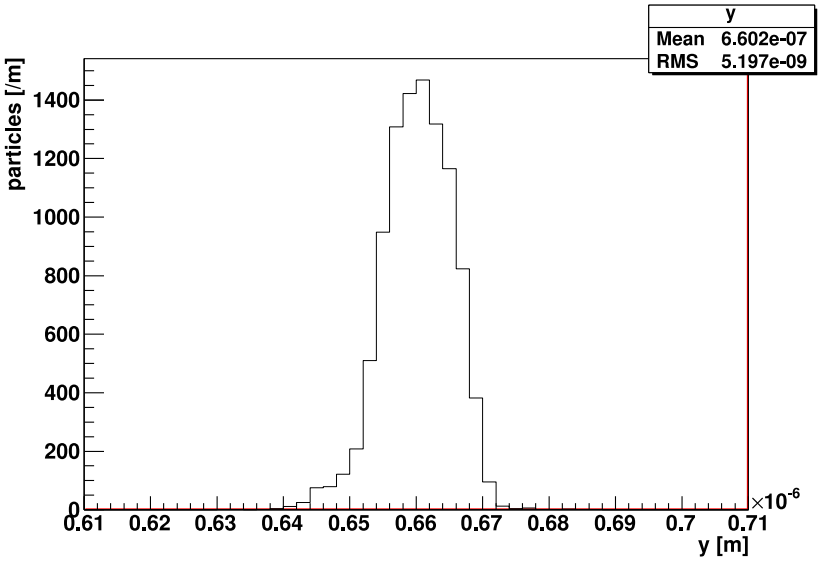


Figure 29: The vertical beam distribution at the IP for the case of a solenoid, an anti-solenoid and synchrotron radiation.

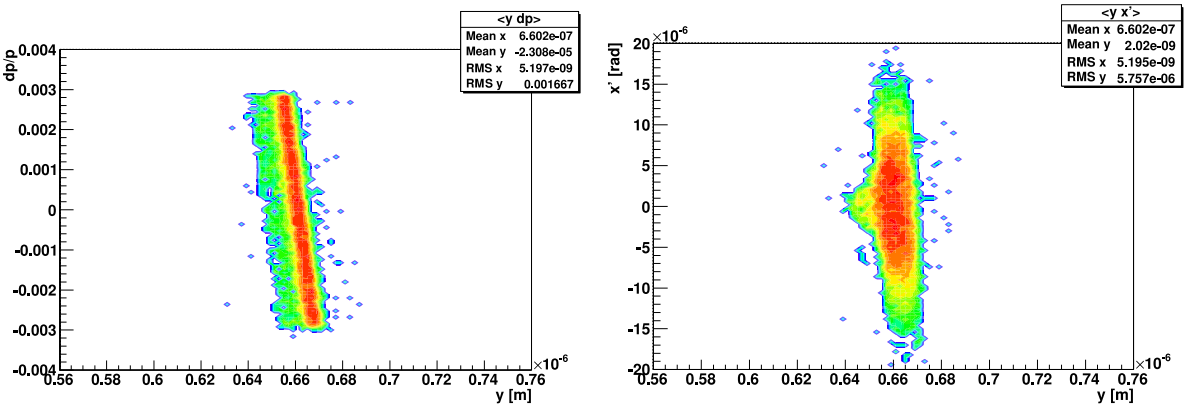


Figure 30: The vertical dispersion (left) and x'-y coupling (right) at the IP for the case of a solenoid, an anti-solenoid and synchrotron radiation.

## 6.4. CONCLUSION

In this note we have studied the impact on the CLIC beam at the IP from the SiD solenoid, and the subsequent correction of these effects with the anti-solenoid. The form of the correction scheme was initially studied in [22], where it was shown that a set of anti-solenoid coils over QD0 corrects the majority of beam aberrations. In this note, we used the newly developed code IRSYN to bench-mark the correction and demonstrate the recovery of the majority of the machine luminosity. The analysis was done with the SiD solenoid and associated anti-solenoid correction coils. The calculation of the interaction region beam dynamics using IRSYN with no solenoid field and no synchrotron radiation shows the expected beam distributions at the interaction point, and shows the expected beam size growth in the presence of synchrotron radiation. This validates and bench-marks the code IRSYN against existing codes, and cross-checks the radiation emission model. In the presence of the

solenoid field alone, the beam dynamics show the beam coupling and orbit motion demonstrated in existing studies, further validating IRSYN and cross-checking the impact of the solenoid on the beam. Finally the studies performed with the solenoid and the anti-solenoid demonstrate the correction of the orbit and coupling terms by the anti-solenoid. The correction leaves behind a small amount of beam aberration at the IP, which is pre-correctable using the beam delivery system [22].

In conclusion, the code IRSYN has been developed and benchmarked against existing studies of the SiD solenoid in the CLIC interaction region. The level of correction obtained with IRSYN agrees expectations, demonstrating the role of the anti-solenoid.

## 7. REFERENCES

[1] Daniel Schulte. "*Guinea Pig*". http://www-project.slac.stanford.edu/lc/bdir/programs/guinea_pig/gp_index.html.
[2] B. Dalena. private communication.
[3] A. Ferrari et al. "*Conceptual design of a beam line for post-collision extraction and diagnostics at the multi-TeV Compact Linear Collider*". In: Phys. Rev. ST Accel. Beams 12 (2 2009), p. 021001. doi: 10.1103/PhysRevSTAB.12.021001. http://link.aps.org/doi/10.1103/PhysRevSTAB.12.021001.
[4] G. Battistoni et al. "The *FLUKA code: Description and benchmarking*". In: Proceedings of the Hadronic Shower Simulation Workshop 2006. Vol. 896. AIP Conference Proceeding, 2007, pp. 31-49.
[5] A. Ferrari et al. "*FLUKA: a multi-particle transport code*". In: CERN-2005-10 (2005). INFN/TC 05/11, SLAC-R-773.
[6] BDSIM. http://www.pp.rhul.ac.uk/twiki/bin/view/JAI/BdSim.
[7] S. Agostinelli et al. "*Geant4|a simulation toolkit*". In: Nuclear Instruments and Methods in Physics Research Section A: Accelerators, Spectrometers, Detectors and Associated Equipment 506.3 (2003), pp. 250 {303. issn: 0168-9002. doi: 10.1016/S0168 - 9002(03 ) 01368 - 8.
[8] GEANT4. http://geant4.cern.ch/
[9] SB2009 proposal document: http://ilc-edmsdirect.desy.de/ilc-edmsdirect/file.jsp?edmsid=D00000000900425
[10] M.Ross, N. Walker, A. Yamamoto et al, "International Linear Collider Reference Design Report, Volume 3 Accelerator", ILC-REPORT-2007-001. http://ilcdoc.linearcollider.org/
[11] J. Jones & D. Angal-Kalinin, "Beam Delivery System Dogleg Design and Integration for the International Linear Collider", Proceedings of IPAC2010, Kyoto, Japan

[12] D. Angal-Kalinin, “ILC Beam Delivery System lattice design changes since the RDR”, http://projects.astec.ac.uk/ilcdecks/, November 2010.
[13] P.Raimondi and A.Seryi, Phys. Rev. Lett.**86**, 3779-3782
[14] ATF collaboration, http://atf.kek.jp/collab/ap/
[15] ATF2 Proposal, SLAC-R-771, 2005.
[16] G. White et al, Proceedings of PAC2009.
[17] A. Scarfe et al, Proceedings of PAC2009.
[18] Present status and first results of the final focus beam line at the KEK Accelerator Test Facility, P Bambade et al (ATF Collaboration), Phys Rev Special Topics 13 (4) (2010)
[19] A. Scarfe, Ph.D. Thesis “TUNING AND ALIGNMENT OF ATF2”, December 2011.
[20] G. White et al., “ATF2 SUMMARY AND STATUS”, ICFA Beam Dynamics Newsletter, No. 54, 2011
[21] http://newsline.linearcollider.org/2013/05/02/demonstrating-the-ilc-final-focus-parameters/
[22] Y. Nosochkov and A. Seryi, Phys. Rev. Spec. Top. - Acc. Beams **8**, 02001 (2005)
[23] B. Dalena, D. Schulte and R. Tomas, Impact of the Experiment Solenoid on the CLIC Luminosity Proceeding of the 1st International Particle Accelerators Conference 23-28 May 2010, Kyoto, Japan, IPAC10-WEPE029. CLIC-Note-831
[24] D. Swodoba, B. Dalena and R. Tomas CLIC spectrometer magnet interference computation of transversal B-field on primary beam CLIC-Note-815.
[25] R.B. Appleby, N. Bernhard et al, The proceedings of IPAC 2011.
[26] R.B. Appleby, L. Thompson et al, The proceedings of IPAC 2011.
[27] H. Burkhardt, LEP note 632, \Monte Carlo Generator for Synchrotron Radiation", LEP Note 632, CERN, December, 1990.
[28] D. Schulte et al. CERN/PS 2001-028
[29] CLIC Conceptual Design Report, http://project-clic-cdr.web.cern.ch/project-clic-cdr/CDR_Volume1.pdf
[30] ILC Technical Design Report, to be published in 2013.

# 8. FUTURE PLANS / CONCLUSION / RELATION TO OTHER EUCARD WORK

The EuCARD project provided valuable contributions to the CLIC Conceptual Design Report [29] and ILC Technical Design Report [30]. Our participation in ATF2 experimental programme till 2010 made us aware of many beam dynamics and instrumentation challenges which will need to consider when the future linear collider project gets a go ahead.

# ANNEX: GLOSSARY

| Acronym | Definition |
|---|---|
| ILC | International Linear Collider |
| CLIC | Compact LInear Collider |
| IP | Interaction point |
| PCL | Post Collision Line |
| BDS | Beam Delivery System |
| ATF2 | Accelerator Test Facility 2 |
| TME | Theoretical Minimum Emittance |
| FFS | Final Focus System |
| BPM | Beam Position Monitor |